corrosion and materials degradation

MDPI

Article

Corrosion Behavior of Ti and Ti6Al4V Alloy in Brackish Water, Seawater, and Seawater Bittern

Ladislav Vrsalović [1,*], Senka Gudić [1], Antonia Talijančić [1], Jelena Jakić [1], Jure Krolo [2] and Iman Danaee [3]

[1] Faculty of Chemistry and Technology, University of Split, Ruđera Boškovića 35, 21000 Split, Croatia; senka.gudic@ktf-split.hr (S.G.); antonia.talijancic@ktf-split.hr (A.T.); jelena.jakic@ktf-split.hr (J.J.)
[2] Faculty of Electrical Engineering, Mechanical Engineering and Naval Architecture, University of Split, Ruđera Boškovića 32, 21000 Split, Croatia; jkrolo@fesb.hr
[3] Abadan Faculty of Petroleum Engineering, Petroleum University of Technology, Abadan 631, Iran; danaee@put.ac.ir
* Correspondence: ladislav@ktf-split.hr; Tel.: +385-21-329435

Abstract: Ti and Ti6Al4V alloy are extensively utilized in structural parts in engineering applications and the production of medical implants due to their excellent mechanical properties, lightweight, and high corrosion resistance. This study comprehensively evaluates their corrosion behavior in three challenging aquatic environments: brackish water, seawater, and seawater bittern. Utilizing open circuit potential (E_{OC}) measurements with polarization techniques (linear and potentiodynamic) and electrochemical impedance spectroscopy (EIS) measurements, the research highlights distinct environmental influences on corrosion performance. Notably, Ti and Ti6Al4V alloy demonstrated exceptional stability with the highest polarization resistance and lowest corrosion current in brackish water, while seawater bittern presented the most demanding condition for Ti6Al4V. Additionally, the analysis of the electrode surfaces after polarization measurements using optical microscopy, optical profilometry, and SEM/EDS tests revealed minor damage, indicating the high corrosion resistance of these materials. This study advances the understanding of Ti and Ti6Al4V alloy performance in diverse environments and offers valuable insights for optimizing their use in harsh aquatic conditions, particularly for applications requiring durability and longevity.

Keywords: titanium; Ti6Al4V alloy; corrosion; electrochemical methods; surface investigation

Citation: Vrsalović, L.; Gudić, S.; Talijančić, A.; Jakić, J.; Krolo, J.; Danaee, I. Corrosion Behavior of Ti and Ti6Al4V Alloy in Brackish Water, Seawater, and Seawater Bittern. *Corros. Mater. Degrad.* **2024**, *5*, 641–656. https://doi.org/10.3390/cmd5040031

Academic Editor: Cuie Wen

Received: 12 November 2024
Revised: 9 December 2024
Accepted: 16 December 2024
Published: 19 December 2024

1. Introduction

Titanium and its alloys have unique qualities of high strength, low density, excellent corrosion resistance, and biocompatibility, making them a promising material for various engineering applications, especially in the aerospace, automotive, shipbuilding, and biomedical fields [1–5]. Titanium is known for its high corrosion resistance, thanks to the formation of the protective film composed of titanium dioxide (up to 10 nm thickness) that remains stable in a wide range of media. When the passive layer is damaged, the base metal is exposed to oxygen-rich corrosive solutions, causing the dissolved Ti ions to react with oxygen and rapidly form a new oxide film. This new film once again separates the base metal from the corrosive agent, demonstrating the self-healing nature of the passive film. This means titanium alloys can withstand exposure to natural waters and salt solutions, including chlorides, sulfates, silicates, phosphates, nitrates, and carbonates, across a wide pH range [5–8]. Titanium demonstrated lower susceptibility to stress corrosion in chloride solutions compared to stainless steels, making it well suited for water, seawater, and brine applications [9,10]. Moreover, reports confirmed its immunity to general corrosion up to 260 °C, along with a high resistance to erosion and cavitation corrosion up to 36 m/s in marine environments [11]. Ti6Al4V alloy is the most used titanium alloy that exhibits superior mechanical properties compared to commercially pure titanium, featuring a high

strength-to-weight ratio, high fracture toughness, increased corrosion resistance, excellent biocompatibility, and minimal thermal expansion [12–15].

These properties make titanium and Ti6Al4V alloy desirable construction materials for a variety of applications involving seawater, starting from thin-walled heat exchanger tubing, which has good heat transfer properties, up to submarine hulls, ships, platforms, desalination plants, salt production evaporators, and water jet propulsion systems.

The properties of the protective oxide film (nature, composition, and thickness) depend on the environmental conditions. In some conditions, when the integrity of the oxide film is broken, titanium could become vulnerable in a corrosion environment [16].

Mansfield et al. [17] investigated seawater movement's effect on stainless steel and titanium corrosion behavior using a rotating disk electrode. They found that both materials have very low corrosion rates, and that mass transport had no effect on the corrosion rates of these materials due to the presence of a tenacious passive oxide layer. The passive current density was independent of the transport of solution constituents while the cathodic reaction was under charge transport control. Palraj and Venkatachari [18] studied the effect of macrofouling on the corrosion of titanium by impedance and polarization techniques. The results showed negligible Ti corrosion in seawater exposure with an appreciable fouling load. Rao found an increased susceptibility to pitting corrosion of titanium due to exposure to a sulfate-reducing bacteria (SRB) culture [19]. The investigation of Nady [20] revealed that the barrier layer resistance decreases in NaCl polluted with H_2S, indicating that sulfides affect the corrosion behavior of Ti and its alloys. Titanium grade 2 tubes, subjected to a natural seawater environment within heat exchangers, failed, owing to hydrogen-assisted corrosion (HAC) [21].

Su et al. conducted a comprehensive investigation into the corrosion behavior of the wrought Ti-6Al-3Nb-2Zr-1Mo (Ti80) alloy in artificial seawater with varying fluoride ion (F^-) concentrations and pH values. Their findings underscore the significant influence of solution pH on the cathodic and anodic processes, as well as the pronounced promoting effect of fluoride ion concentration on the anodic reaction [22].

Ionic species present in seawater, such as Cl^-, Br^-, F^-, I^-, $HCO_3{}^-$, Ca^{2+}, and dissolved O_2, may be involved in the formation reactions of passive film or its dissolution by its penetration into the film or deposition on its surface. Therefore, they can affect the passivation performance of Ti alloys [10].

This paper combined classical electrochemistry techniques, along with surface analysis testing to compare the corrosion behavior of titanium (Ti) and Ti6Al4V alloy in brackish water, seawater, and seawater bittern, which represents the residue in the saltern during NaCl salt production. The selection of three different media—brackish water, seawater, and seawater bittern—was used to investigate the corrosion behavior of Ti and Ti-6Al-4V alloy in a realistic environment. Assessing corrosion behavior in localized or site-specific environmental conditions, such as seawater with unique salinity, pH, or organic content, can provide novel insights. Research often needs more data on specific regional waters, like brackish waters in estuaries or specific seawater compositions. Seawater bittern is far less explored, but in some industries, like salt production by sun evaporation (e.g., Solana Pag), the seawater bittern is commonly present in large quantities. Due to such water's generally more corrosive behavior, the industry is interested in utilizing more corrosive resistance alloys such as titanium alloys. Furthermore, these alloys are already widely used as a structural part in desalination plants, shipbuilding, the offshore oil and gas industry, heat exchangers, salt production, diving equipment, etc. [9,23–27]. Titanium and its alloys are known as "marine metals" as they represent ideal materials for producing structural parts for seawater desalination facilities and power plants [9,28]. Although stainless steel and copper–nickel alloys are less expensive alternatives, the long-lasting results analysis of the operation of piping systems made of different materials for a significant number of civil fleet ships and vessels has proved that systems made of conventional materials (copper base alloys, stainless steels) have a restricted lifetime, which is significantly less compared to one made of Ti and Ti6Al4V alloy. In some cases, the equipment made from Ti and Ti

alloys (pipes, valve pumps, heat exchangers) had a service life of 40 years [23,29]. Extended service life can result in significant life cycle cost savings. Moreover, the amount of Ti used in production pipeline systems in tankers is several times less than that of copper alloys and steels. Thus, the cost of titanium parts provided for the complete service life is lower than stainless steel or copper–nickel alloys [23].

The other benefit and novelty of this research is comparing Ti with the most used titanium alloy, Ti-6Al-4V, in different corrosive environments, which can reveal how alloying elements can influence corrosion behavior.

2. Results and Discussion

2.1. Electrochemical Measurements

Figure 1 shows the open circuit potential evaluation for Ti (a) and Ti6Al4V alloy (b) in different electrolytes.

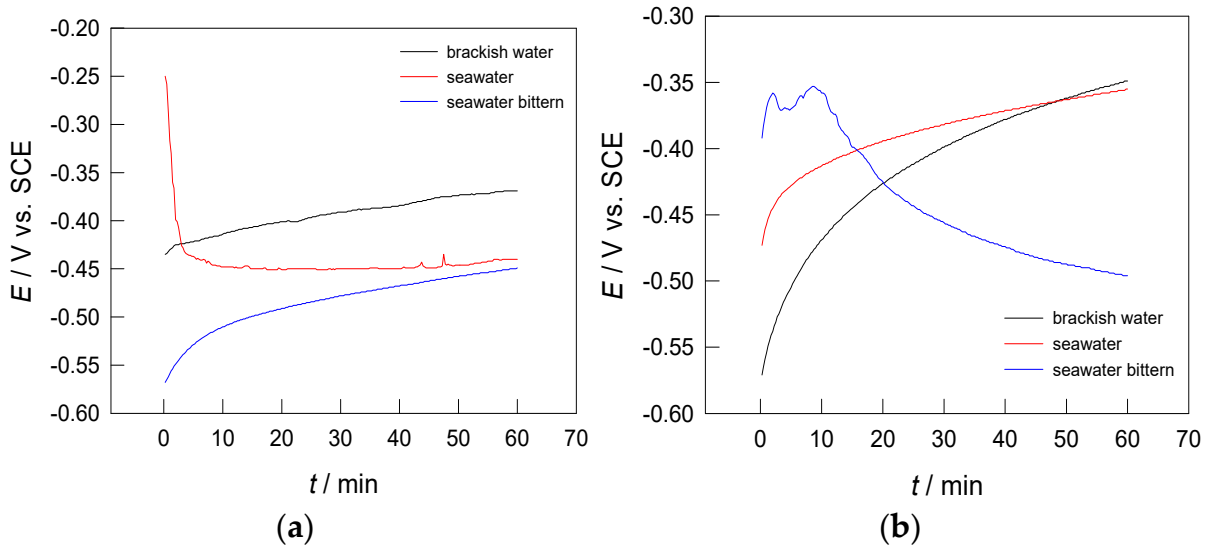

Figure 1. Open circuit potential measurements in brackish water, seawater, and seawater bittern for Ti (**a**) and Ti6Al4V alloy (**b**).

Figure 1a shows that the most negative initial potential is measured for Ti in seawater bittern, where its value has a positive inclination throughout the entire measurement period. A positive change in the E_{OC} was also observed when measuring brackish water, while seawater has a visible initial drop in potential, but then it stabilizes. The most positive E_{OC} value was recorded for the brackish water measurement, while the final E_{OC} values for seawater and brackish water were similar. After immersing the Ti6Al4V electrode in the electrolyte, the potential becomes positive with time for brackish and seawater, and the potential becomes negative for seawater bittern (Figure 1b). At the end of the measurement (after 60 min), similar E_{OC} values were obtained for the Ti6Al4V electrode in brackish and seawater, while a more negative value was observed for the measurement in the seawater bittern.

Figure 2 shows the results of the linear polarization measurements in different electrolytes for titanium (a) and Ti6Al4V alloy (b).

The values of polarization resistance (R_p) shown in Table 1 are determined from the slope of the shown linear *i-E* dependencies. High values of R_p were obtained for all three media, which indicates a high corrosion resistance of Ti in the tested media. The highest R_p value Ti is shown in brackish water, and the lowest is in seawater, which contains the highest concentration of chloride ions. Higher R_p values were obtained in linear polarization investigations of Ti6Al4V in brackish water and seawater compared to pure Ti. However, the Ti6Al4V alloy shows the lowest value of R_p in seawater bittern, which

is most likely a consequence of the high concentration of various cations and anions that negatively affect the corrosion resistance of the alloy.

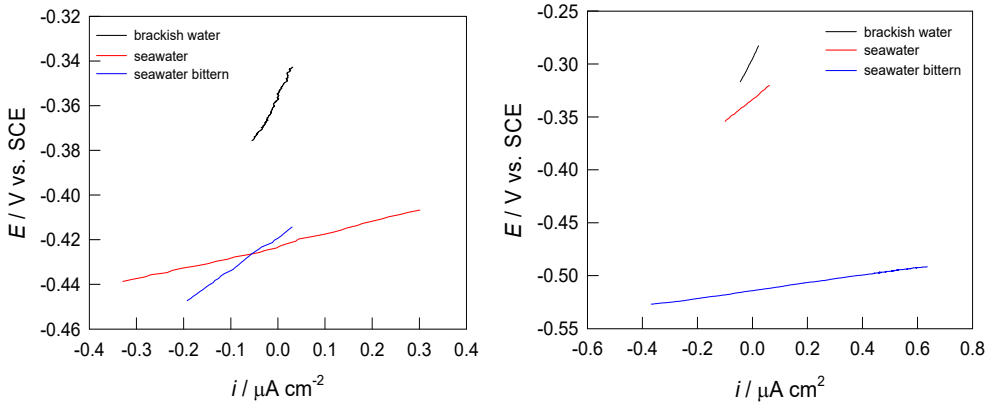

Figure 2. Linear parts of *i-E* curves for Ti (**a**) and Ti6Al4V alloy (**b**) in brackish water, seawater, and seawater bittern.

Table 1. The corrosion parameters of Ti and Ti6Al4V alloy in different electrolytes.

Medium	i_{corr} (μA cm^{-2})	E_{corr} (V)	R_p (kΩ cm^2)
	Ti		
brackish water	0.3	−0.405	413.00
seawater	1.6	−0.455	52.24
seawater bittern	1.2	−0.600	147.00
	Ti6Al4V		
brackish water	0.15	−0.413	511.56
seawater	0.9	−0.585	208.81
seawater bittern	2.2	−0.628	36.75

Potentiodynamic polarization curves in different electrolytes for titanium (a) and Ti6Al4V alloy (b) are shown in Figure 3.

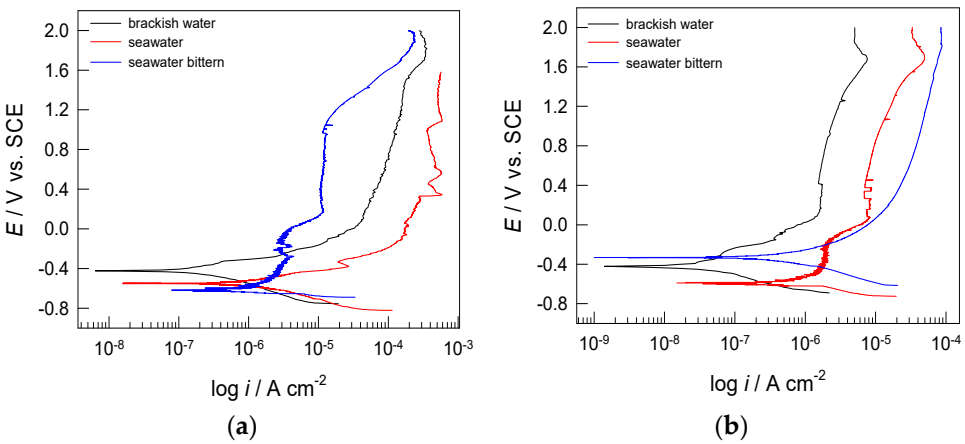

Figure 3. Potentiodynamic potential measurements in brackish water, seawater, and seawater bittern for Ti (**a**) and Ti6Al4V alloy (**b**).

A significant difference in the anodic branches of the curve is visible, which is a consequence of the different intensities of anodic dissolution reactions depending on the medium. The curve obtained by testing seawater bittern shows the lowest anodic current

density. Although the concentration of cations and anions in this electrolyte is the highest, the lower content of the chloride ions compared to the brackish water and seawater is the most likely reason for this behavior. On the other hand, the highest values of anodic current densities were obtained during testing in seawater, which is also related to the highest concentration of chloride ions in the electrolyte. Also, the shape of the anodic curve is different for investigations in the seawater bittern compared to investigations in the brackish water and seawater. Namely, at potentials more positive than the corrosion potential, the anodic part of the curve in seawater bittern is significantly steeper compared to the anodic parts of the curve in brackish water and seawater, which indicates passivation of the electrode surface with a passivation current density of 1 to 10 μm cm^{-2}. When measuring in brackish water, after the corrosion potential, the current increases to a potential of approximately −0.1 V, after which the current does not significantly increase with the changes in potential in a positive direction, which indicates the formation and growth of a protective oxide layer on the surface. A similar phenomenon is also recorded in the polarization curve in the seawater, but with somewhat higher values of anodic current densities. Despite this, it should be noted that at high anodic potentials, anodic current densities did not exceed the value of 5 mA, and there is no indication of reaching breakdown potential. Regarding the potentiodynamic polarization curves for the Ti6Al4V alloy, similar anodic and cathodic behavior is visible, characterized by low values of anodic and cathodic current densities and thus low values of corrosion current densities. The phenomenon of passivity is also characteristic of the Ti6Al4V alloy, which can be seen from the anodic parts of the polarization curves. However, unlike Ti, significantly higher anodic current densities were obtained in measurements in seawater bittern, which shows that high cation and anion concentrations significantly negatively impact the alloy's corrosion resistance. Corrosion parameters were obtained from electrochemical measurements and shown in Table 1.

It can be seen that Ti and Ti6Al4V alloy have the most positive corrosion potential in brackish water, but the most negative in seawater bittern. Furthermore, for Ti, the lowest value of the corrosion current density was recorded in brackish water, but the highest in seawater. While for the Ti6Al4V alloy, the highest corrosion current density was recorded in seawater bittern. Corrosion current density values are generally low in all three media, along with high polarization resistance values, indicating high Ti and Ti6Al4V alloy corrosion resistance.

According to Zhang et al. [30], the mechanism of electrochemical reactions of Ti corrosion in seawater can be described as follows:

$$Ti \rightarrow Ti^{2+} + 2e^{-} \quad (1)$$

The Ti^{2+} ion is unstable in water and forms a Ti^{3+} ion, which transforms into $Ti(OH)_3$ according to the following reactions:

$$2Ti^{2+} + 2H_2O \rightarrow 2Ti^{3+} + 2OH^{-} + H_2 \quad (2)$$

$$Ti^{3+} + 3OH^{-} \rightarrow Ti(OH)_3 \quad (3)$$

$Ti(OH)_3$ turns into TiO_2 according to the following reaction (4):

$$2Ti(OH)_3 \rightarrow 2TiO_2 \cdot 2H_2O + H_2 \quad (4)$$

According to various authors [26,31,32], the surface oxide layer on the Ti6Al4V alloy dominantly contains TiO_2, which is formed first, considering that Ti has a higher affinity for bonding with oxygen compared to Al and V, which is formed according to the following reaction (5):

$$Ti + O_2 \rightarrow TiO_2 \quad (5)$$

The reaction of oxygen and aluminum leads to the formation of Al_2O_3, which is also detected on the surface of the Ti6Al4V alloy in the form of Al-rich regions [5,12,33].

$$4Al + 3O_2 \rightarrow 2Al_2O_3 \quad (6)$$

Vanadium is the last to react with oxygen, forming V_2O_5 according to the following reaction (7):

$$4V + 5O_2 \rightarrow 2V_2O_5 \quad (7)$$

Vanadium cannot be detected at the outermost surface in natural oxides; it is located below the top surface and may only be observed after some sputtering either by XPS or AES [34].

The EIS results also confirm the extent of surface reactivity of the tested samples under open circuit conditions. The results for cp-Ti and Ti6Al4V in different chloride media are shown in Figure 4 in the Nyquist and Bode diagrams.

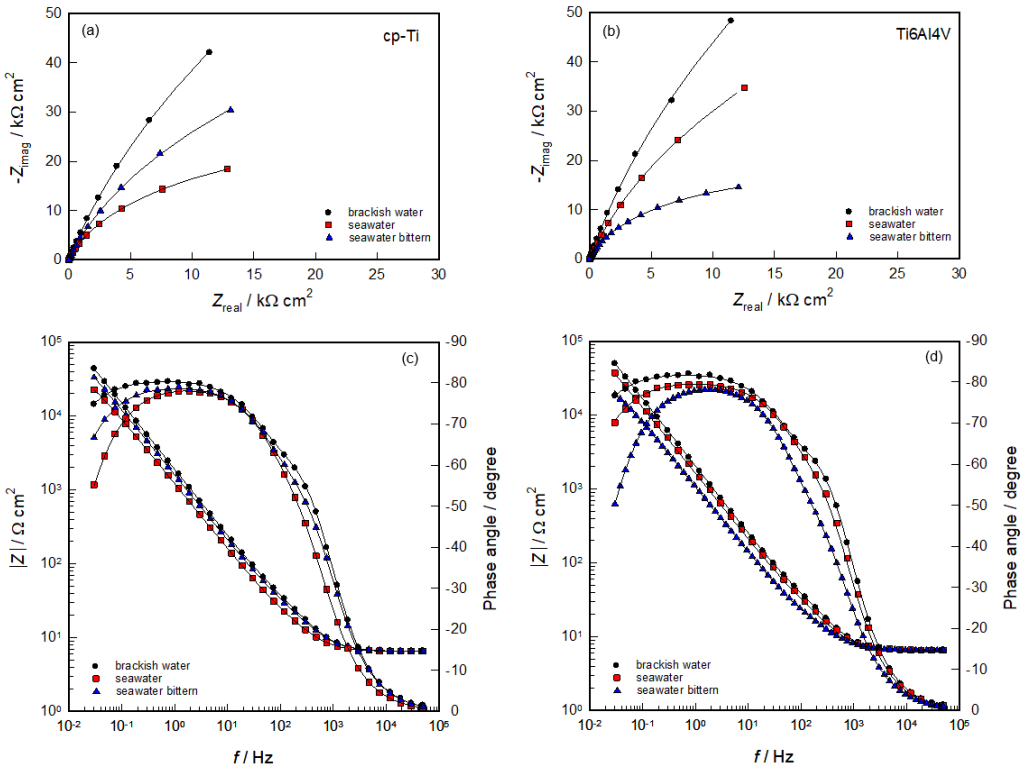

Figure 4. Nyquist (**a**,**b**) and Bode (**c**,**d**) plots recorded on cp-Ti and Ti-6Al-4V alloy in different solutions.

In the Nyquist diagram, incomplete capacitive semicircles can be seen, indicating that the investigated systems have extremely high resistance (impedance) due to the passive nature of the surface films [16,30,35]. For both samples, the size and radius of the semicircles significantly depend on the type of electrolyte.

The Bode plane represents the impedance and phase angle dependence on the frequency (log |Z|—log f; phase shift—log f). In the high-frequency range, only the influence of the electrolytic resistance, R_{el}, was observed in the total impedance, with a phase shift of $\approx 0^\circ$. In the medium and low-frequency range, a double capacitive behavior is observed for both samples, reflecting the dielectric properties of the surface protection layer. The total impedance of the system (as well as the phase shift) also depends on the type of electrolyte used. For the Ti sample, |Z| increases in the following order: seawater < seawater bittern < brackish water. For the Ti6Al4V alloy, |Z| increases in the following order: seawater bittern < seawater < brackish water.

The results obtained are consistent with the data found in the literature. It is widely recognized that the oxide film on the surface of Ti and its alloys has a two-layer structure, comprising an inner, thin, compact layer known as the barrier film and an outer, porous layer [30–38]. The inner barrier film exhibits an exceptionally high impedance, whereas the outer porous layer demonstrates significantly lower impedance.

Figure 5 presents the equivalent circuit (EC) used to analyze the impedance data. It includes the electrolyte resistance, R_{el} (3–8 Ω cm^2), connected in series with two-time constants. The high-frequency time constant (Q_1R_1) represents the properties of the porous (outer) part of the oxide film; R_1 is the resistance of the porous layer (i.e., the resistance of the electrolyte inside the pores) while Q_1 describes the capacitance of the porous layer. The medium/low-frequency time constant (Q_2R_2) describes the inner, i.e., barrier part of the oxide film, where R_2 represents the resistance, and Q_2 *is* the capacitance of the inner layer.

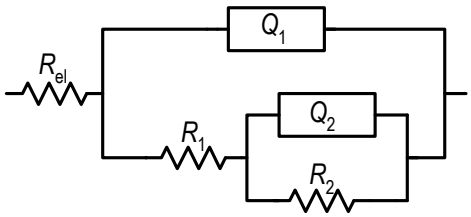

Figure 5. The EC model used to fit the EIS data.

According to the size of the coefficients n_1 and n_2, the constant phase elements (CPEs; Q_1 and Q_2) in the EC represent the deviation of the capacitance (C) from the ideal behavior [39]. The calculated EC parameters are listed in Table 2. The Q was transformed in C using the following equation [22,40,41]:

$$C = \left[QR^{1-n}\right]^{1/n} \tag{8}$$

Table 2. Electrical parameters of equivalent circuit obtained by fitting EIS data for cp-Ti and Ti6Al4V in different solutions.

Medium	$Q_1 \times 10^6$ (Ω^{-1} s^n cm^{-2})	n_1	C_1 (μF cm^{-2})	R_1 (Ω cm^2)	$Q_2 \times 10^6$ (Ω^{-1} s^n cm^{-2})	n_2	C_2 (μF cm^{-2})	d_2 (nm)	R_2 (kΩ cm^2)
				Ti					
brackish water	61.57	0.87	28.90	100.23	39.32	0.87	42.84	2.00	414.96
seawater	110.91	0.85	46.28	62.27	50.75	0.85	56.27	1.52	53.48
seawater bittern	78.45	0.85	31.81	74.76	44.99	0.86	48.54	1.77	148.30
				Ti6Al4V					
brackish water	56.78	0.87	26.79	112.65	34.32	0.89	36.53	2.35	508.54
seawater	73.83	0.86	32.36	86.32	40.28	0.86	43.87	1.96	208.09
seawater bittern	121.16	0.85	48.57	45.41	61.39	0.83	65.36	1.31	37.48

And the obtained values for the porous and barrier layers (C_1, C_2) are also provided in Table 2.

After one h of immersion in chloride media, both samples show good protective properties due to the inner part of the oxide layer (R_2 is three orders of magnitude higher than R_1). It is also important to note that the sum of the resistances (R_1 + R_2) represents the polarization resistance (R_p) of the system [22], and these results agree with those of the polarization measurements. The higher the polarization resistance, the higher the corrosion resistance of the system. From the data in the table, R_1 and R_2 (and their sum) for the Ti samples increase in the order of seawater < seawater bittern < brackish water, while for the Ti6Al4V alloy, the order is as follows: seawater bittern < seawater < brackish water.

In both samples, the increase in the resistance of the barrier and porous layers (R_1, R_2) is accompanied by a corresponding decrease in their capacities (C_1, C_2). In addition, the capacitance of the porous layer is lower than the capacitance of the barrier layer under all test conditions (regardless of the type of sample and medium). Based on the plate capacitor model, the capacitance of the oxide film is inversely proportional to its thickness, d, as follows:

$$C = \frac{\varepsilon_o \varepsilon}{d} \quad (9)$$

where ε_o represents the permittivity of vacuum, and ε is the dielectric constant of the oxide film. Considering that the oxide film on Ti and Ti6Al4V mainly consists of TiO_2, whose dielectric constant is 100 according to the literature [40,41], the thickness of the barrier layer was roughly estimated, and the obtained results are given in Table 2.

As mentioned, the resistance of the porous layer on Ti and Ti alloy in all tested solutions is relatively low (compared to the barrier layer), suggesting that the pores in the oxide film are likely filled with the electrolyte solution. Due to its open structure, determining the thickness of the outer porous layer is difficult. From these findings, it can be concluded that the corrosion of both samples is primarily prevented by the thin inner barrier layer (≈2 nm) of high resistance (≈from 40 to 500 kΩ cm^2). Furthermore, according to the results given in the table, the thickness, polarization resistance, and thus the corrosion resistance of Ti and Ti6Al4V samples are highest in brackish water. In contrast, Ti in seawater and the alloy Ti6Al4V in seawater bittern show the poorest corrosion resistance (lowest thickness and polarization resistance), which is consistent with the polarization measurements.

2.2. Surface Analysis

Immediately after the potentiodynamic polarization measurements were completed, the electrodes were taken out of the electrochemical cell and immersed in a beaker with deionized water. After 1 min, they were removed and dried by a stream of warm air. The dry surfaces of the electrodes were examined with a light microscope at a magnification of 100 times. The results are shown in Figure 6 for Ti electrodes and Ti6Al4V electrodes.

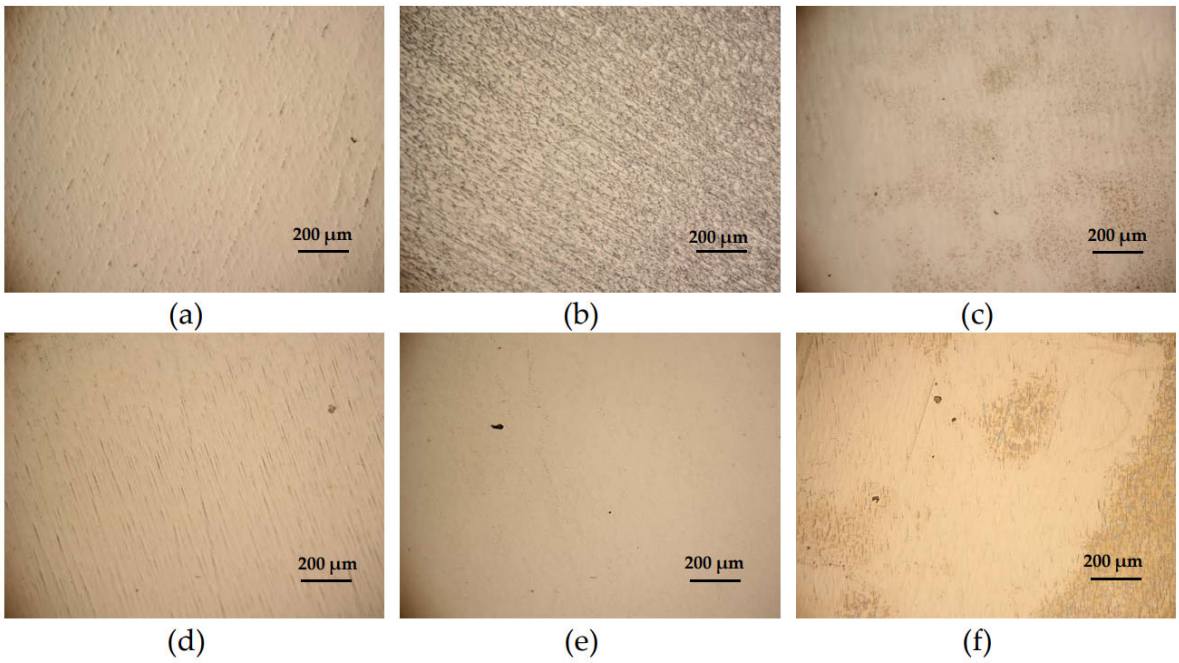

Figure 6. Optical microscope images of surface of Ti after potentiodynamic polarization measurements in (**a**) brackish water, (**b**) seawater, and (**c**) seawater bittern; and surfaces of Ti6Al4V after measurements in (**d**) brackish water, (**e**) seawater, and (**f**) seawater bittern.

Barely noticeable damages are visible on the electrode surfaces, with the most significant changes observed on the surface of the Ti electrode after the polarization tests carried out in seawater, where the highest values of anodic current densities were also achieved. The images of the surface also show clear and slight markings that remained after the manual mechanical preparation of the electrode by grinding and polishing. Similar surface conditions can also be seen on the Ti6Al4V alloy, where minor damages are most noticeable on the electrode exposed to seawater bittern.

SEM/EDS analysis can provide better insight into the Ti and Ti6Al4V surface condition after potentiodynamic polarization tests were conducted. Figure 7 shows SEM images of the Ti and Ti6Al4V surfaces after polarization measurements, which confirmed the electrochemical measurements regarding the highest corrosion attack on Ti in seawater and on Ti6Al4V in seawater bittern.

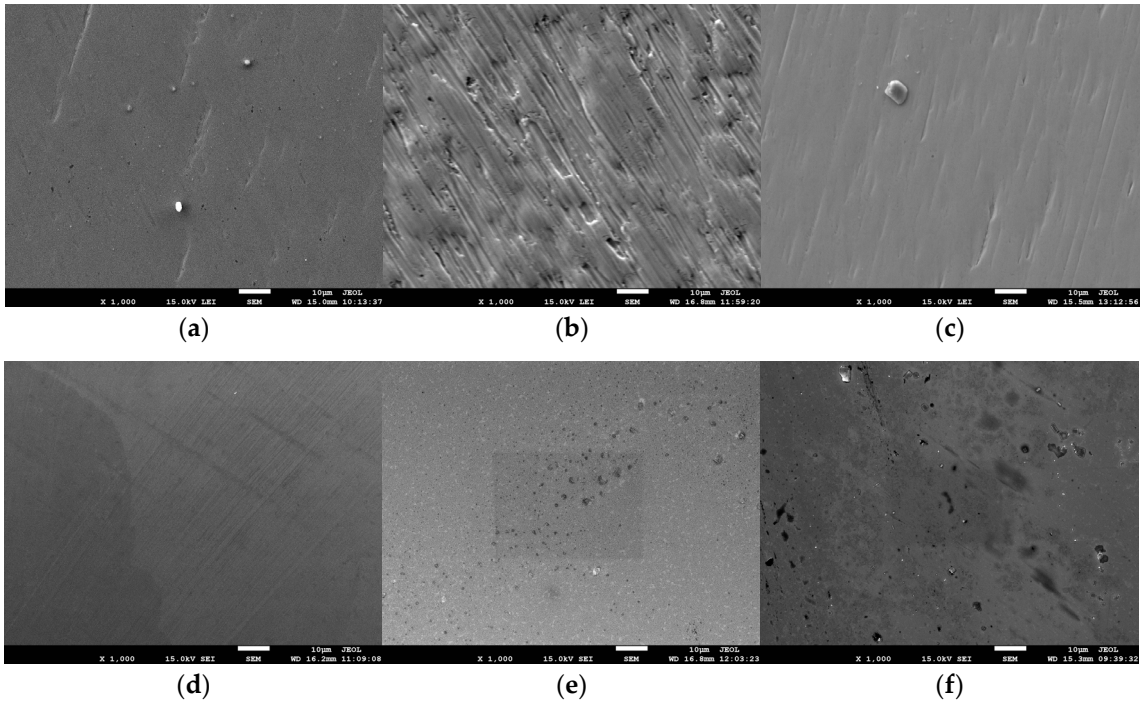

Figure 7. SEM images of surface of Ti after potentiodynamic polarization measurements in (**a**) brackish water, (**b**) seawater, and (**c**) seawater bittern; and surfaces of Ti6Al4V after measurements in (**d**) brackish water, (**e**) seawater, and (**f**) seawater bittern.

EDS analysis was performed on the Ti surface, which was exposed to seawater, and on the Ti6Al4V alloy exposed to seawater bittern during polarization measurements, and the results are shown in Figures 8 and 9 and Tables 3 and 4.

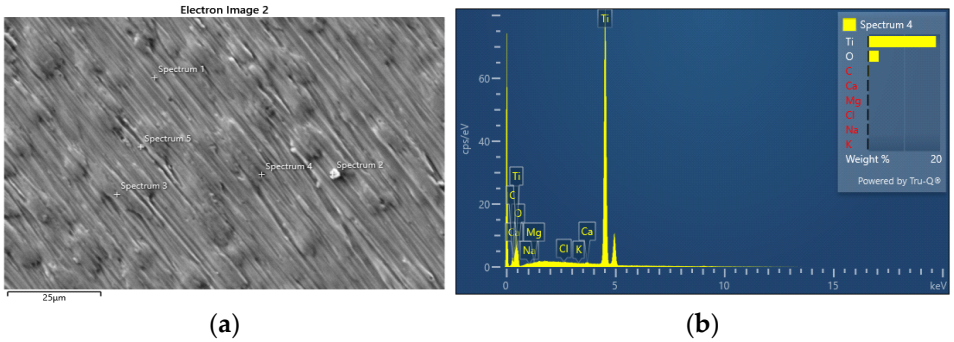

Figure 8. (**a**) SEM image of surface of Ti after potentiodynamic polarization measurements in seawater and (**b**) EDS point analysis in Spectrum 4.

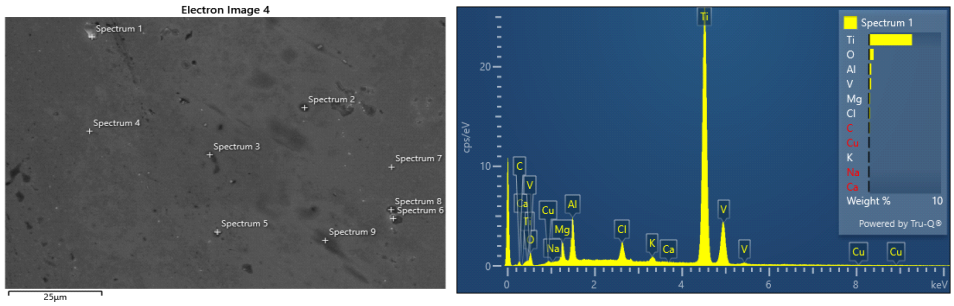

(**a**) (**b**)

Figure 9. (**a**) SEM image of surface of Ti6Al4V after potentiodynamic polarization measurements in seawater bittern and (**b**) EDS point analysis in Spectrum 1.

Table 3. EDS elemental analysis at different positions of Ti sample after polarization measurement in seawater.

Elements (wt%)	Spectrum 1	Spectrum 2	Spectrum 3	Spectrum 4	Spectrum 5
O	11.05	8.63	10.78	13.45	9.17
Na	-	-	-	-	-
Mg	-	-	-	0.05	-
Al	0.44	0.28	0.28	-	0.38
Cl	-	-	-	-	-
K	-	-	-	-	-
Ca	0.05	0.38	0.10	0.22	-
Ti	87.94	90.25	88.83	86.28	90.00
Cu	0.53	0.46	-	-	0.45
Si	-	-	0.11	-	-

Table 4. EDS elemental analysis at different positions of Ti6Al4V sample after polarization measurement in seawater bittern.

Elements (wt%)	Spectrum 1	Spectrum 2	Spectrum 3	Spectrum 4	Spectrum 5	Spectrum 6	Spectrum 7	Spectrum 8	Spectrum 9
O	8.64	13.58	8.92	5.77	26.27	7.78	6.67	13.31	6.76
Na	-	-	-	-	-	0.12	-	0.08	-
Mg	2.14	2.47	0.59	-	0.86	1.07	-	0.24	0.45
Al	4.24	4.86	5.63	6.23	8.15	5.24	5.59	5.21	5.76
Cl	2.11	1.07	0.28	-	0.64	0.84	-	0.27	0.22
K	0.74	0.26	-	-	0.15	0.22	-	-	-
Ca	-	0.04	0.15	0.07	-	0.06	-	0.43	-
Ti	77.30	72.41	80.43	84.10	60.75	81.18	82.67	76.93	82.16
V	4.04	4.30	3.14	3.02	2.52	3.32	4.07	3.43	3.76
Cu	0.78	0.86	0.67	0.81	0.66	-	1.0	-	0.90
S	-	0.14	0.15	-	-	0.17	-	0.12	-

Numerical data shown in Table 3 reveal a high percentage of Ti in all positions. The second dominant element is oxygen, the percentage of which changes depending on the position, ranging from about 9.17 to 11.05%. Other elements appear sporadically in certain positions at a significantly smaller percentage. The appearance of copper is most likely related to the use of a conductive copper strip that covered a small part of the metal surface for gaining the electrical contact between the electrode and the support necessary for SEM/EDS measurements, given that the polyacrylate insulating mixture is non-conductive.

Table 4 shows that the alloying elements of the Ti6Al4V alloy show the highest elemental percentage. As expected, oxygen is present in a relatively high percentage at every

point, followed by chlorine and other elements in smaller percentages, as seawater bittern has the highest concentration of dissolved ions.

Figure 10 shows 3D optical profilometry measurements. Optical profilometry was used as the non-contact and user-friendly method for maximizing surface investigation and also offers the advantages of combined 2D and 3D capability. The Profilm3D optical profiler (KLA Corporation, Milpitas, CA, USA) uses white light interferometry, which enables measures of the surface profiles and roughness down to 0.05 µm, which makes it a useful device for surface degradation and topography measurement after corrosion measurement techniques. It also enables the measurement of the area surface roughness according to the ISO 25178 height standard [42], which is a step forward from the usual line surface roughness measurements.

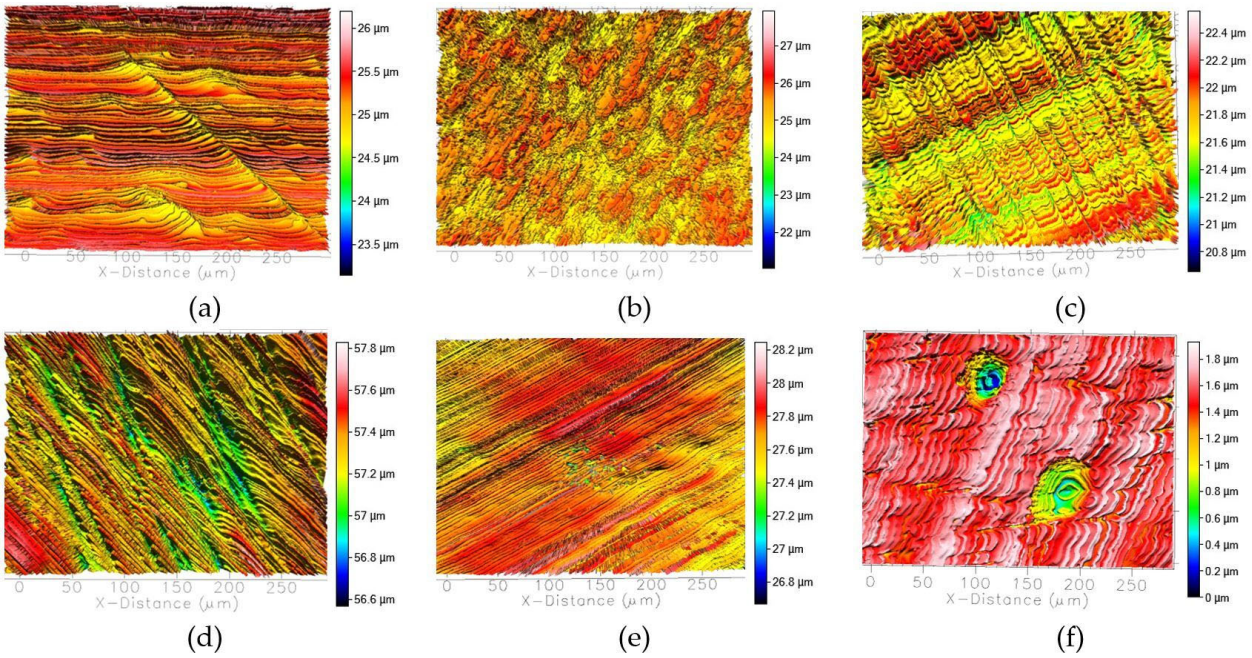

Figure 10. Three-dimensional optical profilometry images of surface of = Ti after potentiodynamic polarization measurements in (**a**) brackish water, (**b**) seawater, and (**c**) seawater bittern; and surfaces of Ti6Al4V after measurements in (**d**) brackish water, (**e**) seawater, and (**f**) seawater bittern.

In this case, 3D optical profilometry was used as a tool to evaluate area surface roughness (Sa) since, due to the excellent corrosion resistance of Ti electrodes, there were no significant corrosion pits at the used profilometry scanning resolution. According to the 3D profilometry results and Figure 10a–c, the Ti electrode mean arithmetic surface roughness values for brackish water, seawater, and seawater bittern were 0.1704 µm, 0.386 µm, and 0.1585 µm, respectively. Therefore, the maximum value of surface roughness of the Ti electrode was obtained by measurement in seawater, which also corresponds to the highest values of corrosion current density and lowest corrosion potential values, Table 1. The surface roughness increment indicates pronounced corrosion development, which confirms potentiodynamic polarization measurements. According to Figure 10d–f and the 3D profilometry results for Ti6Al4V, the electrode mean arithmetic surface roughness values for brackish water, seawater, and seawater bittern were 0.1147 µm, 0.08973 µm, 0.1354 µm, respectively. In this case, the maximum surface roughness of the Ti6Al4V electrode was obtained by measurement in seawater bittern, which also corresponds to the highest corrosion current density and lowest corrosion potential values, as shown in Table 1.

Overall, the surface roughness for the Ti6Al4V electrode is smaller than for the Ti electrode, which indicated generally better corrosion resistance, which is also confirmed with

the potentiodynamic polarization measurements. However, the highest corrosion current density and lowest corrosion potential values were obtained at the Ti6Al4V electrode in seawater bittern, as shown in Table 1. According to Figures 10f and 11, that is also the only specimen where corrosion pits were developed, which indicated different corrosion mechanisms in these specimens in seawater bittern due to the different chemical composition than in pure Ti electrodes. It is fair to say that despite increased corrosion resistance and the preserved surface of the Ti6Al4V electrode compared with the Ti electrode in sea and brackish water, there is a significant deterioration of both surface appearance and corrosion resistance of the Ti6Al4V electrode in seawater bittern, as shown in Figure 11 and Table 1. According to Figure 11, the visible corrosion pits have a width of 50–80 µm, while the depth is only 1.5 µm. Therefore, the obtained surface pits are relatively wide but very shallow.

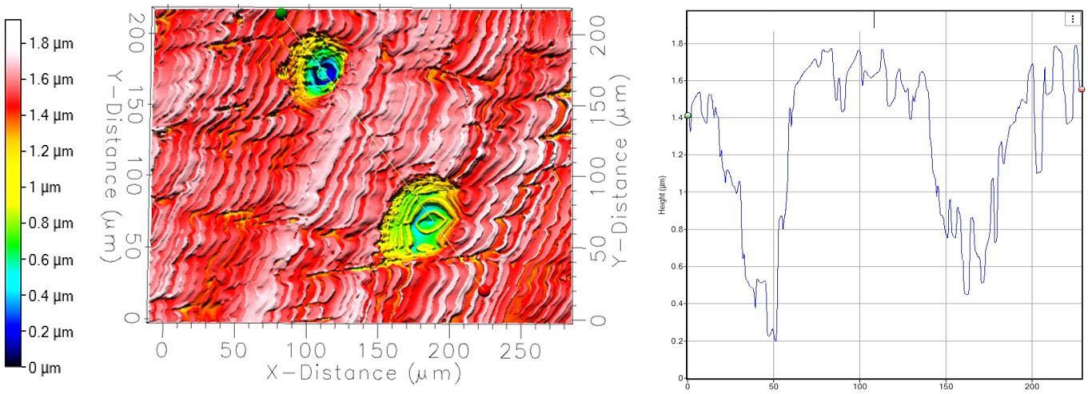

Figure 11. Three-dimensional appearance of corrosion pits and line profile measurement for Ti6Al4V electrode after potentiodynamic polarization measurements in seawater bittern.

3. Materials and Methods

A sample of 99.6% pure titanium and a titanium alloy with 6% aluminum and 4% vanadium (Ti6Al4V) in the form of rods were purchased from GoodFellow Cambridge Ltd. (Huntingdon, UK). Both rods were 20 cm long, with a diameter of 0.4 cm for Ti and 0.5 cm for the Ti6Al4V alloy rod. From the original samples, three smaller pieces in the shape of a cylinder with a length of 1.5 cm were cut with a metallographic cutter Buehler Delta Abrasimet (Buehler, Lake Bluff, IL, USA). The connection between the base of the cylinder and the insulated copper wire was achieved by pulse welding using the Lampert PUK U5 device (Lamper Werktechnik GmbH, Werneck, Germany). After joining, the electrodes were protected from all sides, except for one (the opposite base of the cylinder in relation to the connection point with the Cu wire), with epoxy resin (Presi, Eybens, France), whereby the non-insulated bases of the Ti cylinder (surface area 0.125 cm^2) and the cylinder Ti6Al4V alloy (surface area 0.196 cm^2) represented working surfaces that were in contact with the electrolyte. The investigations were carried out in three different electrolytes: brackish water, seawater, and seawater bittern. Brackish water was collected in Solin near the city of Split, where the Jadro River flows into the Adriatic Sea, while the seawater was collected in the village of Stobreč near Split. Seawater bittern was collected from a slattern in Ramova (Krvavica–Makarska, Croatia). Seawater bittern is a highly concentrated and very bitter-tasting solution that remains after the evaporation and crystallization of NaCl from brines and seawater during sea salt production. The chemical composition of seawater bittern was shown elsewhere [43].

The physical characteristics of the electrolyte are determined by a portable device with a YSI PRO 1030 measuring probe (Xylem Inc., Yellow Springs, OH, USA) and shown in Table 5.

Table 5. Physical characteristics of electrolytes.

Medium	pH	Conductivity (mS cm^{-1})	Density (g cm^{-3})	Salinity (ppt)	TDS
brackish water	7.90	21.3	1.025	6.1 ppt	7.01
seawater	7.89	43.6	1.030	29.9 ppt	29.99
seawater bittern	6.21	133.3	1.305	69 ppt *	62.3 *

* The values marked with (*) for seawater bittern were obtained after 5-time dilution with deionized water.

As seawater bittern is a highly concentrated ionic solution, salinity and TDS measurements are impossible without dissolution because the values exceed the upper measuring limit of the YSI PRO 1030 measuring probe. Therefore, a 5-time dissolution was performed to determine salinity and TDS values. The corrosion investigation was conducted with undiluted seawater bittern.

Mechanical preparation of the surface of the working electrodes prior to electrochemical measurement was carried out using a Metkon Forcipol 1V metallographic grinder/polisher (Metkon, Bursa, Turkey) by wet grinding with sandpapers of fineness 180, 400, 600, 800, 1200, and 2500, after which the surfaces were polished with a polishing suspension (Presi alumina suspension 0.3 μm). This was followed by ultrasonic cleaning in ethanol for 4 min and in deionized water for 4 min in an ASonic Pro ultrasonic bath (ASonic, Ljubljana, Slovenia) to remove any remaining particles from the work surface.

The electrochemical measurements were performed in a 200 mL double-wall glass electrochemical cell with a Pt-mesh counter-electrode and a saturated calomel electrode (SCE) as the referent electrode. All potentials in this paper are referred to the SCE. The temperature of the solution was maintained at a constant 24 °C, a crucial factor for accurate measurements, using a Huber Kiss thermostatic bath (Huber, Offenbourg, Germany). The measurements were carried out using a PAR 273A potentiostat/galvanostat coupled to the PAR M5210 lock-in amplifier (Princeton Applied Research, Oak Ridge, TN, USA) in the following set:

- Monitoring of the open circuit potential (E_{OC}) for 60 min in which the value of the potential is recorded every 15 s;
- Electrochemical impedance spectroscopy measurement in a frequency range of 30×10^{-3} Hz to 50×10^{3} Hz with the AC amplitude of 10 mV;
- Linear polarization method, in the potential range of ±20 mV according to E_{OC} (v = 0.2 mV s^{-1});
- Potentiodynamic polarization method, in the potential area from −0.400 V to 2.0 V (v = 1 mV s^{-1}).

Following the electrochemical tests, the electrode surfaces were subjected to a comprehensive analysis. The optical microscope MXFMS-BD, Ningbo Sunny Instruments Co., China (Ningbo, China), and the optical profilometer Filmetrics Profilm 3D, KLA Company (Milpitas, CA, USA) were used to provide a detailed understanding of the surfaces. Additionally, an SEM/EDS analysis of the surface was conducted using a scanning electron microscope JEOL JSM 7610F Plus (Jeol Ltd., Tokyo, Japan).

4. Conclusions

Ti and Ti6Al4V alloys exhibit high corrosion resistance in the tested media, evidenced by low values of corrosion currents and high values of polarization resistance. These findings have the potential to significantly inform and empower material selection for specific environments, enhancing the effectiveness and longevity of engineering projects.

The highest values of polarization resistance and the lowest values of corrosion current of Ti and the Ti6Al4V alloy were found in tests in brackish water. The greatest difference in behavior was observed in tests in seawater bittern, where Ti had the lowest anodic current

densities. The highest values of corrosion current density, anodic current densities, and the lowest values of polarization resistance were found for the Ti6Al4V alloy.

EIS measurements indicated that the oxide film on the surface has a two-layer structure, and the barrier part of the oxide film successfully prevents corrosion processes.

Examination of the electrode surface by optical and SEM microscopy after the polarization measurements revealed small surface damages, which, in the case of Ti, were most pronounced on the surface of the electrode immersed in a sea line, but in the case of the Ti6Al4V alloy, after the polarization measurements in seawater bittern.

After polarization measurements in seawater bittern, the optical profilometry showed that surface roughness for the Ti6Al4V electrode is smaller than for the Ti electrode in brackish water and seawater, which indicated generally better corrosion resistance, which is also confirmed with the potentiodynamic polarization measurements. However, the highest corrosion current density and lowest corrosion potential values of all samples were obtained at the Ti6Al4V electrode in seawater bittern, where there were also relatively wide but distinctly shallow pits on the surface of the Ti6Al4V alloy. No significant surface damage was observed on the other surfaces. This indicates that possibly different corrosion mechanisms occurred in Ti6Al4V electrode in seawater bittern water due to the different chemical composition than in pure Ti electrodes.

Author Contributions: Conceptualization, L.V., S.G. and A.T.; methodology, L.V. and S.G.; software, L.V., S.G., J.K. and J.J.; validation, S.G., J.J. and I.D.; formal analysis, A.T., L.V. and S.G.; investigation, A.T., J.J. and J.K.; resources, L.V. and S.G.; writing—original draft preparation, L.V., S.G., J.K. and I.D.; writing—review and editing, L.V., S.G., J.K. and I.D.; visualization, S.G., L.V., J.K., A.T. and J.J.; supervision, L.V. and S.G.; project administration, L.V. and S.G.; funding acquisition, L.V. All authors have read and agreed to the published version of the manuscript.

Funding: This research received no external funding.

Data Availability Statement: The data presented in this study are available on request from the corresponding author.

Conflicts of Interest: The authors declare no conflicts of interest.

References

1. Haile, F.; Adkins, J.; Corradi, M. A review of the use of titanium for reinforcement of masonry structures. *Materials* **2022**, *15*, 4561. [CrossRef]
2. Najafizadeh, M.; Yazdi, S.; Bozorg, M.; Mehran, G.-M.; Hosseinzadeh, M.; Zarrabian, M.; Cavaliere, P. Classification and applications of titanium and its alloys: A review. *J. Alloys Compd. Commun.* **2024**, *3*, 100019. [CrossRef]
3. Torbati-Sarraf, H.; Ding, L.; Khakpour, I.; Daviran, G.; Poursaee, A. Unraveling the corrosion of the Ti–6Al–4V orthopedic alloy in phosphate-buffered saline (PBS) solution: Influence of frequency and potential. *Corros. Mater. Degrad.* **2024**, *5*, 276–288. [CrossRef]
4. Lunde, L.; Seiersten, M. Offshore Application for titanium alloys. In *Titanium and Titanium Alloys: Fundamentals and Applications*; Leyens, C., Peters, M., Eds.; Wiley-VCH Verlag GmbH and Co.: Darmnstad, Germany, 2003; pp. 483–496. [CrossRef]
5. Gudić, S.; Vrsalović, L.; Kvrgić, D.; Nagode, A. Electrochemical behaviour of Ti and Ti-6Al-4V alloy in phosphate buffered saline solution. *Materials* **2021**, *14*, 7495. [CrossRef] [PubMed]
6. Thorhallsson, A.I.; Karlsdottir, S.N. Corrosion behaviour of titanium alloy and carbon steel in a high-temperature, single and mixed-phase, simulated geothermal environment containing H_2S, CO_2 and HCl. *Corros. Mater. Degrad.* **2021**, *2*, 190–209. [CrossRef]
7. Takadoum, J. Review on corrosion, tribocorrosion and osseointegration of titanium alloys as biomaterials. *Corros. Mater. Degrad.* **2023**, *4*, 644–658. [CrossRef]
8. Yang, J.; Song, Y.; Dong, K.; Han, E.-H. Research progress on the corrosion behavior of titanium alloys. *Corros. Rev.* **2023**, *41*, 4–20. [CrossRef]
9. Wang, C.P.; Wang, H.Z.; Ruan, G.L.; Wang, S.H.; Xiao, Y.X.; Jiang, L.D. Applications and prospects of titanium and its alloys in seawater desalination industry. *IOP Conf. Ser. Mater. Sci. Eng.* **2019**, *688*, 033036. [CrossRef]
10. Yan, S.; Song, G.-L.; Li, Z.; Wang, H.; Zheng, D.; Cao, F.; Harynova, M.; Dargusch, M.S.; Zhou, L. A state of-the-art review on passivation and biofouling of Ti and its alloys in marine environments. *J. Mater. Sci. Technol.* **2018**, *34*, 421–435. [CrossRef]
11. Prando, D.; Brenna, A.; Pedeferri, M. Corrosion of Titanium: Part 1: Aggressive environments and main forms of degradation. *J. Appl. Biomater. Func.* **2018**, *15*, 291–302. [CrossRef]
12. Cvijović-Alagić, I.; Cvijović, Z.; Bajat, J.; Rakin, M. Composition and processing effects on the electrochemical characteristics of biomedical titanium alloys. *Corros. Sci.* **2014**, *83*, 245–254. [CrossRef]

13. Elshaer, R.N.; Ibrahim, K.M. Study of microstructure, mechanical properties, and corrosion behavior of as-cast Ni-Ti and Ti-6Al-4V alloys. *J. Mater. Eng. Perform.* **2023**, *32*, 7831–7845. [CrossRef]
14. Ghisheer, M.M.M.; Esen, I.; Ahlatci, H.; Akın, B. Investigation of microstructure, mechanics, and corrosion properties of Ti6Al4V alloy in different solutions. *Coatings* **2024**, *14*, 277. [CrossRef]
15. Naghavi, S.H.R.; Wang, H.; Varma, S.N.; Tamaddon, M.; Marghoub, A.; Galbraith, R.; Galbraith, J.; Moazen, M.; Hua, J.; Xu, W.; et al. On the morphological deviation in additive manufacturing of porous Ti6Al4V scaffold: A design consideration. *Materials* **2022**, *15*, 4729. [CrossRef] [PubMed]
16. Yang, X.; Du, C.; Wan, H.; Liu, Z.; Li, X. Influence of sulfides on the passivation behavior of titanium alloy TA2 on simulated seawater environments. *Appl. Surf. Sci.* **2018**, *458*, 198–209. [CrossRef]
17. Mansfield, F.; Liu, G.; Xiao, H.; Tsai, C.H.; Little, B.J. The corrosion behavior of copper alloys, stainless steels and titanium in seawater. *Corros. Sci.* **1994**, *36*, 2063–2095. [CrossRef]
18. Palraj, S.; Venkatachari, G. Effect of biofouling on corrosion behavior of grade 2 titanium in Mandapam seawaters. *Desalination* **2008**, *230*, 92–99. [CrossRef]
19. Rao, T.S.; Kora, A.J.; Anupkumar, B.; Narasimhan, S.V.; Feser, R. Pitting corrosion of titanium by a freshwater strain of sulphate reducing bacteria (*Desulfovibrio vulgaris*). *Corros. Sci.* **2005**, *47*, 1071–1084. [CrossRef]
20. Nady, H.; El-Rabiei, M.M.; Samy, M. Corrosion behavior and electrochemical properties of carbon steel, commercial pure titanium, copper and copper–aluminum–nickel alloy in 3.5% sodium chloride containing sulfide ions. *Egypt. J. Pet.* **2016**, *26*, 79–94. [CrossRef]
21. Yang, Z.G.; Gong, Y.; Yuan, J.Z. Failure analysis of leakage on titanium tubes within heat exchangers in a nuclear power plant. Part I: Electrochemical corrosion. *Mater. Corros.* **2012**, *63*, 7–17. [CrossRef]
22. Su, B.; Wang, B.; Luo, L.; Wang, L.; Su, Y.; Xu, Y.; Li, B.; Li, T.; Huang, H.; Guo, J.; et al. Corrosion behaviour of a wrought Ti-6Al-3Nb-2Zr-1Mo alloy in artificial seawater with various fluoride concentration and pH values. *Mater. Des.* **2022**, *214*, 110416. [CrossRef]
23. Gorynin, I.V. Titanium alloys for marine application. *Mater. Sci. Eng. A* **1999**, *263*, 112–116. [CrossRef]
24. Shultz, R.W.; Baxter, C.F.; Boster, P.L. Applying titanium alloys in drilling and offshore production systems. *JOM* **2001**, *53*, 33–35. [CrossRef]
25. Gurrappa, I. Characterization of titanium alloy Ti-6Al-4V for chemical, marine and industrial applications. *Mater. Charact.* **2003**, *51*, 131–139. [CrossRef]
26. Chen, W.; Zhang, D.; Wang, E.; Yan, F.; Xiang, L.; Xie, Z. Corrosion degradation of Ti6Al4V alloys in simulated marine environments. *Coatings* **2022**, *12*, 1028. [CrossRef]
27. Froes, F.H. *Titanium Physical Metallurgy Processing and Applications*; ASM International Materials Park: Novelty, OH, USA, 2015.
28. Richaud-Minier, H.; Marchebois, H.; Gerard, P. Titanium and super stainless steel welded tubing solutions for sea water cooled heat exchangers. *Mater. Technol.* **2009**, *24*, 191–200. [CrossRef]
29. Schumerth, D.J. Titanium tubing still going strong after 40 years. *Power* **2011**, *155*, 58–60. Available online: https://www.powermag.com/titanium-tubing-still-going-strong-after-40-years/ (accessed on 10 November 2024.).
30. Zhang, D.; Liu, Y.; Liu, R.; Guan, X.; Xing, S.; Dou, X.; He, Z.; Zhang, X. Characterization of corrosion behavior of TA2 titanium alloy welded joints in seawater environment. *Front. Chem.* **2022**, *10*, 950768. [CrossRef]
31. Shahba, R.M.A.; Ghannem, W.A.; El-Sayed El-Shenawy, A.; Ahmed, A.S.I.; Tantawy, S.M. Corrosion and Inhibition of Ti-6Al-4V Alloy in NaCl Solution. *Int. J. Electrochem. Sci.* **2011**, *6*, 5499–5509. [CrossRef]
32. Casadebaigt, A.; Hugues, J.; Monceau, D. High Temperature Oxidation and Embrittlement at 500–600 °C of Ti-6Al-4V Alloy Fabricated by Laser and Electron Beam Melting. *Corros. Sci.* **2020**, *175*, 108875. [CrossRef]
33. Bocchetta, P.; Chen, L.-Y.; Tardelli, J.D.C.; Reis, A.C.D.; Almeraya-Calderón, F.; Leo, P. Passive Layers and Corrosion Resistance of Biomedical Ti-6Al-4V and β-Ti Alloys. *Coatings* **2021**, *11*, 487. [CrossRef]
34. Neacsu, E.I.; Constantin, V.; Yanushkevich, K.; Donath, C.; Anastasescu, M.; Popescu, M. Surface modification on Ti-6Al-4V alloy during corrosion in high temperature ionic liquid. *Rev. Chem.* **2020**, *71*, 207–219. [CrossRef]
35. Ahmadian, Z.; Danaee, I.; Golozar, M.A. Effect of Surface Treatment on Corrosion Resistance of 304 Stainless Steel Implants in Tyrode Solution. *Arch. Metall. Mater.* **2014**, *59*, 25–30. [CrossRef]
36. Cheng, J.; Li, J.; Yu, S.; Du, Z.; Dong, F.; Zhang, J.; Zhang, X. Corrosion Behavior of As-Cast Ti–10Mo–6Zr–4Sn–3Nb and Ti–6Al–4V in Hank's Solution: A Comparison Investigation. *Metals* **2021**, *11*, 11. [CrossRef]
37. Pan, J.; Thierry, D.; Leygraf, C. Electrochemical impedance spectroscopy study of the passive oxide film on titanium for implant application. *Electrochim. Acta* **1996**, *41*, 1143–1153. [CrossRef]
38. Dai, N.; Zhang, L.C.; Zhang, J.; Zhang, X.; Ni, Q.; Chen, Y.; Wu, M.; Yang, C. Distinction in corrosion resistance of selective laser melted Ti-6Al-4V alloy on different planes. *Corros. Sci.* **2016**, *111*, 703–710. [CrossRef]
39. Barsoukov, E.; Macdonald, J.R. *Impedance Spectroscopy, Theory, Experiment, and Applications*; John Wiley & Sons, Inc.: Hoboken, NJ, USA, 2005.
40. Bai, Y.; Li, S.J.; Prima, F.; Hao, Y.L.; Yang, R. Electrochemical corrosion behavior of Ti-24Nb-4Zr-8Sn alloy in a simulated physiological environment. *Appl. Surf. Sci.* **2012**, *258*, 4035–4040. [CrossRef]

41. Yang, Z.; Yu, M.; Han, C.; Zhao, Z.; Jia, X.; Zhao, M.; Li, S.; Liu, J. Evolution and corrosion resistance of passive film with polarization potential on Ti-5Al-5Mo-5V-1Fe-1Cr alloy in simulated marine environments. *Corros. Sci.* **2023**, *221*, 111334. [CrossRef]
42. Available online: https://www.iso.org/obp/ui/#iso:std:iso:25178:-2:ed-2:v1:en (accessed on 17 December 2024.).
43. Jakic, J.; Jakić, M.; Yousefi, S.; Labor, M. PVA assisted preparation of $Mg(OH)_2$/MgO nanostructures from seawater bittern through precipitation method. *Sadhana* **2024**, *49*, 139. [CrossRef]